Article

Template Synthesis of Cyclometalated Macrocycle Iridium(III) Complexes Based on Photoinduced C−N Cross-Coupling Reactions In Situ

Xiao-Kang Huang, Hai-Yun Zhou,* Gao-Feng Liu, and Bao-Hui Ye*

Read Online

ACCESS | Metrics & More | Article Recommendations | SI Supporting Information

ABSTRACT: The synthesis of metal macrocycle complexes holds paramount importance in coordination and supramolecular chemistry. Toward this end, we report a new, mild, and efficient protocol for the synthesis of cyclometalated macrocycle Ir(III) complexes: $[Ir(L1)](PF_6)$ (**1**), $[Ir(L2)](PF_6)$ (**2**), and $[Ir(L3)]$-(PF_6) (**3**), where **L1** presents 10,17-dioxa-3,6-diaza-2(2,8),7(8,2)-diquinolina-1,8(1,4)-dibenzenacyclooctadecaphane, **L2** is 10,13,16,19,22,25-hexaoxa-3,6-diaza-2(2,8),7(8,2)-diquinolina-1,8-(1,4)-dibenzenacyclohexacosaphane, and **L3** is 4-methyl-10,13,16,19,22,25-hexaoxa-3,6-diaza-2(2,8),7(8,2)-diquinolina-1,8-(1,4)-dibenzenacyclohexacosaphane. This synthesis involves the preassembly of two symmetric 2-phenylquinoline arms into C-shape complexes, followed by cyclization with diamine via in situ interligand C−N cross-coupling, employing a metal ion as a template. Moreover, the synthetic yield of these cyclometalated Ir(III) complexes, tethered by an 18-crown-6 ether-like chain, is significantly enhanced in the presence of K$^+$ ion as a template. The resultant cyclometalated macrocycle Ir(III) complexes exhibit high stability, efficient singlet oxygen generation, and superior catalytic activity for the aerobic selective oxidation of sulfides into sulfoxides under visible light irradiation in aqueous media at room temperature. The photocatalyst **2** demonstrates recyclability and can be reused at least 10 times without a significant loss of catalytic activity. These results unveil a new and complementary approach to the design and in situ synthesis of cyclometalated macrocycle Ir(III) complexes via a mild interligand-coupling strategy.
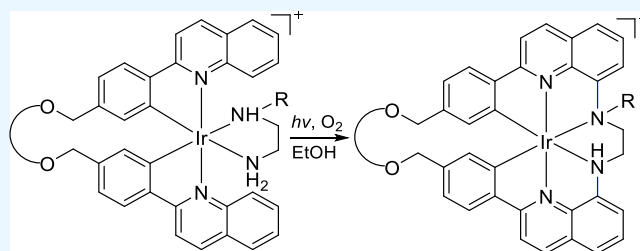
INTRODUCTION

Cyclometalated Ir(III) complexes are extensively utilized in photophysical applications, including organometallic light-emitting diodes (OLEDs) for light harvesting and energy transfer,[1] as luminescent sensors for metal ions and biological labels,[2] and as photocatalysts for electron and energy transfer in catalytic synthesis.[3] Their widespread adoption is attributed to a high phosphorescence quantum yield, large Stoke shifts, and robust chemical and thermal photostability. Traditionally, modulating the emission color and phosphorescence lifetime of Ir(III) emitters has primarily involved structural modifications of the ligands. These modifications encompass alterations in conjugation degree and the incorporation of the electron-donating and electron-withdrawing groups.[1−3] Nevertheless, insights into the influence of ligand topology on the photophysical and photochemical properties of these chromophores remain limited,[4] possibly due to synthetic challenges in fabricating topologically complex cyclometalated iridium complexes. Moreover, polydentate ligands have been extensively harnessed to enhance the phosphorescence properties of metal complexes by bolstering metal−ligand binding strength and enabling thermally accessible metal-centered d−d transitions.[5] A notable strategy is linking two ligands via a bridge. For instance, Lee's group reported a marked increase in

phosphorescence efficiency by connecting ortho-carboranes to the 5 positions of Ir(III) ppy complexes (see Scheme 1A, where ppy is 2-phenylpyridine).[6a] Utilizing a naphthalene linker to connect bis-ppy ligands, they explored its application in white-light emission (see Scheme 1B).[6b] Remarkedly, an Ir(III) complex featuring a C,C,C,C-tetradentate ligand, bridging two bis(1-phenylimidazolium) ligands with a butylene bridge, exhibited blue-green emissions with a high quantum yield of 0.96 (see Scheme 1C).[6c] Additionally, the development of tripodal and cage ligands has further advanced the photophysical properties of Ir(III) emitters.[7,8] In these structures, the metal ion is fully encapsulated by organic ligands, providing enhanced protection from the quenchers. The emission behavior and maximum wavelength of the tripodal Ir(III) complex D (see Scheme 1D) were solvent-independent.[7d] The cage Ir(III) complex E (see Scheme 1E) demonstrated an 80% reduction in oxygen quenching
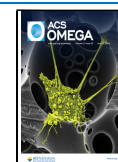
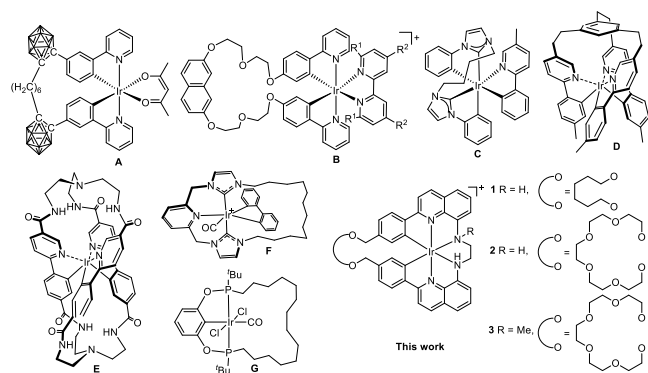**Scheme 1. Diagrams for the Selected Tetradentate (A, B, and C), Tripodal (D), Cage (E), and Macrocycle (F and G) Ir(III) Cycolmetalated Complexes**

compared to the prototypical Ir(ppy)$_3$.[8a] However, the observation of nonplanar cyclometalated macrocycle complex is still scarce.[9] The cyclometalated macrocycle Ir(III) complexes F based on the CNC pincer ligand linking by a flexible dodecamethylene chain (see Scheme 1F)[9b] and G coordinated with the PCP pincer ligand tethering by a tetradecamethylene linker (see Scheme 1G)[9c] have been synthesized and used for catalytic reactions. Remarkable, Wang's group reported the first cyclometalated tetradentate macrocyclic Pt(II) complex, which displays a higher thermal stability and emission quantum efficiency (95% in 10% PMMA film) than the corresponding nonmacrocyclic tetradentate Pt(II) analogues.[9d] Moreover, tetradentate NHC macrocycle Pt(II), Pd(II), Ni(II), and Ru(II) complexes have been also prepared and used as catalysts.[9e−h]

Synthetic macrocycles represent an expanding category of compounds in the realms of supramolecular, material, and biomedical chemistry because of their notable stability.[10] Nonetheless, the development of an efficient and universally applicable methodology for the synthesis of macrocycles remains an enduring challenge, primarily due to the entropic barriers encountered in macrocyclization reactions.[11] The introduction of metal-template synthesis six decades ago, which has proven to be an exceptionally efficacious approach for crafting crown ethers and polyamine macrocycle complexes,[12,13] prompts an inquiry into whether this template-directed methodology could be extended to the synthesis of cyclometalated macrocycle complexes.

Prior investigations from our group have established a robust protocol for the amination of coordinated 2-phenylquinoline (pq) complexes at the C8 position through in situ interligand C−N cross-coupling under visible light irradiation in an oxygen-rich environment.[14,15] Mechanistic explorations revealed that metal aminyl radicals play a pivotal role in forming new C−N bond.[14b,15b] These findings offer a new pathway for the in situ generation of new multidentate complexes. The efficacy and mildness of the reaction conditions for this in situ interligand cross-coupling prompted us to extend this methodology to the synthesis of cyclometalated macrocycle complexes. In the context of our ongoing research, we present the synthesis of three innovative cyclometalated macrocycle Ir(III) complexes: [Ir(**L1**)](PF$_6$) (**1**), [Ir(**L2**)](PF$_6$) (**2**), and [Ir(**L3**)](PF$_6$) (**3**), as depicted in Scheme 1. Here, **L1** is defined as 10,17-dioxa-3,6-diaza-2(2,8),7(8,2)-diquinolina-1,8(1,4)-dibenzenacyclooctadecaphane; **L2** as 10,13,16,19,22,25-hexaoxa-3,6-diaza-2(2,8),7(8,2)-diquinolina-1,8(1,4)-dibenzenacyclo-

hexacosaphane; and **L3** as 4-methyl-10,13,16,19,22,25-hex-aoxa-3,6-diaza-2(2,8),7(8,2)-diquinolina-1,8(1,4)-dibenzenacy-clohexacosaphane. These complexes were synthesized through in situ interligand C−N cross-coupling under benign conditions and served as a locking fragment. This approach provides a facile and complementary protocol for the in situ construction of metal macrocycle complexes via a postcoordination interligand-coupling strategy under mild conditions. Subsequently, we conducted selective photooxidations of sulfide into sulfoxide using these Ir(III) macrocycle complexes as photosensitizers under blue-light irradiation in an O$_2$ atmosphere at room temperature in aqueous media. For comparison, acyclic complexes [Ir(**L4a**)$_2$(en)](PF$_6$) (where **L4a** is 2-(4-(ethoxymethyl)phenyl)quinoline, en is 1,2-ethyl-enediamine) and [Ir(**L4**)](PF$_6$) (where **L4** is N,N′-bis(2-(4-(ethoxymethyl)phenyl)quinolin-8-yl)ethane-1,2-diamine) were also synthesized, and their catalytic properties were evaluated.

■ EXPERIMENTAL SECTION

Materials and Methods. All reagents used in this investigation were commercially available and used without further purification, unless specified otherwise. Detailed synthetic procedures for ligands 1,6-bis((4-(quinolin-2-yl)-benzyl)oxy)hexane (**L1a**) and 1,18-bis(4-(quinolin-2-yl)-phenyl)-2,5,8,11,14,17-hexaoxaoctadecane (**L2a**) are provided in the Supporting Information. The synthesis of ligand **L4a** was executed following previously published protocols.[16] Column chromatography was performed using 300−400 mesh silica gel, with precautions taken to minimize light exposure. Elemental analysis (C, H, and N) was carried out using an Elementar Vario EL analyzer. ^{1}H and ^{13}C nuclear magnetic resonance (NMR) spectra were acquired on a Bruker AV 600 MHz spectrometer, utilizing TMS as internal standards. High-resolution mass spectrometry (HRMS) spectra were recorded on a Thermo Scientific LTQ-XL ion trap mass spectrometer. UV−visible spectra were obtained by using a PerkinElmer Lambda 950 spectrophotometer. Steady-state photolumines-cence spectra were recorded on an Edinburgh Instruments FLS 980 Photoluminescence Spectrometer. Fluorescence lifetimes were ascertained using an IBH 5000F coaxial nanosecond flash lamp. Fluorescence quantum yields were quantified employing the Edinburgh Instruments FLS 1000 Quantum Yield Integrating Sphere Measurement System with PMT980 Detector. Photo-oxidation experiments were performed using a blue-light-emitting diode (LED) corn lamp (λ = 450−470 nm, 80 W) sourced from Shenzhen Nuoguan Technology Co., Ltd. as a light source.

Singlet Oxygen Quantum Yields. The quantum yield Φ_Δ for ^{1}O$_2$ generation in air-saturated MeOH was quantified by monitoring the photo-oxidation of 1,3-diphenylisobenzofur-an (DPBF) sensitized by the Ir(III) complex. The absorbance of DPBF was adjusted to approximately 1.0 at 410 nm in a mixture of air-saturated MeCN/MeOH. The photo-oxidation of DPBF was recorded at 5-s intervals. The quantum yields of singlet oxygen generation (Φ_Δ) were calculated by a relative method using Rose Bengal (RB, Φ_Δ^{std} = 0.76 in air-saturated MeOH) as the reference. The quantum yield Φ_Δ was calculated by the following equation:

$$\Phi_\Delta^{unk} = \Phi_\Delta^{std} \frac{m^{unk} F^{std}}{m^{std} F^{unk}}$$

Here, superscripts unk and std designate Ir complexes and RB, respectively; m is the slope of a plot of the difference in change in absorbance of DPBF (at 414 nm) with the irradiation time, and F is the absorption correction factor, which is given by $F = 1-10^{-A}$ (absorbance at the irradiation wavelength). Experimental error for the reported quantum yield was about 15%.

General Procedure for the Synthesis of [Ir(La)- (MeCN)$_2$](PF$_6$) Complexes (La = L1a, L2a or (L4a)$_2$). Ligands **L1a**, **L2a** (1.25 mmol), or **L4a** (2.50 mmol), IrCl$_3$ (1 mmol), and KCl (2 mmol) were combined in a solution of 2-ethoxyethanol (15 mL) and H$_2$O (5 mL). Then, this reaction mixture was stirred at 120 °C for a prescribed duration under a N$_2$ atmosphere. Upon cooling to room temperature, the reaction mixture was diluted with 30 mL of water, and the resultant product was extracted by CH$_2$Cl$_2$ thrice (3 × 15 mL). The organic phase was consecutively washed with water and brine and then dried over anhydrous Na$_2$SO$_4$. The filtrate was evaporated under reduced pressure and subjected to column chromatography on silica gel, using a CH$_2$Cl$_2$/CH$_3$OH mixture (100/3, v/v) as the eluent, to isolate the red products [Ir(La)Cl]$_2$. Subsequently, the [Ir(La)Cl]$_2$ was dissolved in 20 mL of CH$_3$CN and stirred at 80 °C overnight. After cooling to room temperature, 20 mL of CH$_2$Cl$_2$ was added, and the solution was washed with a saturated KPF$_6$ solution (3 × 15 mL). The organic phase was dried in anhydrous Na$_2$SO$_4$ and filtered. The filtrate was evaporated to yield [Ir(La)(MeCN)$_2$]- (PF$_6$).

[Ir(L1a)(MeCN)$_2$](PF$_6$). Yield 35% for 24 h. HRMS Calcd. [C$_{38}$H$_{34}$IrN$_2$O$_2$]$^+$, m/z = 743.22440. Found: 743.22504 [M-2MeCN-PF$_6$]$^+$. ^{1}H NMR (600 MHz, DMSO-d_6) δ 8.96 (d, J = 8.9 Hz, 2H), 8.73−8.68 (m, 2H), 8.50 (d, J = 8.8 Hz, 2H), 8.17 (d, J = 7.9 Hz, 2H), 7.99 (d, J = 7.9 Hz, 2H), 7.86 (t, J = 7.5 Hz, 2H), 7.76−7.70 (m, 2H), 6.90−6.86 (m, 2H), 5.96 (s, 2H), 4.16 (d, J = 12.2 Hz, 2H), 3.60−3.57 (m, 2H), 2.97−2.92 (m, 2H), 2.66−2.61 (m, 2H), 1.24 (s, 6H), 0.94−0.90 (m, 2H), 0.81−0.77 (m, 2H), 0.46 (d, J = 12.5 Hz, 2H), 0.42−0.37 (m, 2H). ^{13}C NMR (151 MHz, DMSO) δ 170.12, 170.12, 148.85, 148.85, 146.47, 146.47, 142.04, 142.04, 140.85, 140.85, 139.85, 139.85, 135.59, 135.59, 131.73, 131.73, 130.10, 130.10, 129.18, 129.18, 127.96, 127.96, 127.27, 127.27, 126.78, 126.78, 126.67, 126.67, 123.79, 123.79, 117.75, 117.75, 72.49, 72.49, 67.04, 67.04, 29.48, 29.48, 29.14, 29.14, 24.15, 24.15.

[Ir(L2a)(MeCN)$_2$](PF$_6$). Yield 85% for 6 h. HRMS Calcd. for [C$_{42}$H$_{42}$IrN$_2$O$_6$]$^+$, m/z = 863.26666. Found: 863.26678 [M-2MeCN-PF$_6$]$^+$. ^{1}H NMR (600 MHz, DMSO-d_6) δ 9.07−9.04 (m, 2H), 8.69 (d, J = 8.6 Hz, 2H), 8.48−8.43 (m, 2H), 8.17 (d, J = 7.8 Hz, 2H), 7.96 (d, J = 7.9 Hz, 2H), 7.86 (t, 2H), 7.73 (t, 2H), 6.92−6.88 (m, 2H), 6.02 (s, 2H), 4.14−4.11 (m, 2H), 3.95 (d, J = 12.5 Hz, 2H), 3.36−3.34 (m, 10H), 3.25−3.20 (m, 10H), 1.24 (s, 6H). ^{13}C NMR (151 MHz, DMSO-d_6) δ 170.15, 170.15, 148.88, 148.88, 146.21, 146.21, 141.66, 141.66, 140.76, 140.76, 140.24, 140.24, 133.23, 133.23, 131.69, 131.69, 129.17, 129.17, 128.05, 128.05, 127.22, 127.22, 126.94, 126.94, 126.77, 126.77, 121.89, 121.89, 117.72, 117.72, 116.72, 116.72, 72.06, 72.06, 70.23, 70.23, 70.23, 70.23, 70.23, 70.23, 69.95, 69.95, 69.27, 69.27, 29.34, 29.34.

[Ir(L4a)$_2$(MeCN)$_2$](PF$_6$). Yield 80% for 24 h. HRMS Calcd. for [C$_{36}$H$_{32}$IrN$_2$O$_2$]$^+$, m/z = 717.20875. Found: 717.20911 [M-2MeCN-PF$_6$]$^+$. ^{1}H NMR (600 MHz, DMSO-d_6) δ 9.10 (d, J = 8.7 Hz, 2H), 8.71−8.69 (m, 2H), 8.47−8.45 (m, 2H), 8.18−8.16 (m, 2H), 7.95 (d, J = 8.0 Hz, 2H), 7.87 (s, 2H), 7.74 (t, 2H), 6.79 (d, J = 7.8 Hz, 2H), 6.08 (s, 2H), 4.05 (d, J = 21.8 Hz, 4H), 3.04 (s, 2H), 2.99 (d, J = 9.0 Hz, 2H), 0.70 (t,

12H). ^{13}C NMR (151 MHz, DMSO-d_6) δ 170.09, 170.09, 148.92, 148.92, 146.12, 146.12, 141.79, 141.79, 140.81, 140.81, 140.49, 140.49, 132.74, 132.74, 132.74, 132.74, 131.70, 131.70, 129.14, 129.14, 128.15, 128.15, 127.22, 127.22, 126.89, 126.89, 126.81, 126.81, 121.35, 121.35, 117.68, 117.68, 71.32, 71.32, 64.97, 64.97, 15.16, 15.16, 15.16, 15.16.

General Procedure for the Synthesis of [Ir(La)(en)]- (PF$_6$) Complexes. To synthesize [Ir(La)(en)](PF$_6$) complexes, [Ir(La)(MeCN)$_2$](PF$_6$) (0.05 mmol) was introduced into a 10-mL CH$_2$Cl$_2$ solution containing either en or N-methyl-1,2-ethylenediamine (men) (0.12 mmol). The solution was stirred at room temperature under a N$_2$ atmosphere for 6 h. Subsequently, an additional 20 mL of CH$_2$Cl$_2$ was added, followed by washing with a saturated KPF$_6$ solution (3 × 15 mL). The organic layer was then dried in anhydrous Na$_2$SO$_4$ and filtered. The resulting filtrate was concentrated under reduced pressure and subjected to column chromatography on silica gel, using a CH$_2$Cl$_2$/CH$_3$OH/Et$_3$N (100/2/0.005, v/v/ v) mixture as the eluent. This process yielded the desired Ir(III) diamine complexes as pale red powder.

[Ir(L1a)(en)](PF$_6$) (1a). Yield: 96%. Anal. Calcd. for C$_{40}$H$_{42}$F$_6$IrN$_4$O$_2$P: C 50.68, H 4.47, N 5.91. Found: C 50.36, H 4.74, N 5.69. HRMS Calcd. for [C$_{40}$H$_{42}$IrN$_4$O$_2$]$^+$, m/z = 803.29263. Found: 803.29425 [M-PF$_6$]$^+$. ^{1}H NMR (600 MHz, CD$_3$CN) δ 8.51 (d, J = 8.8 Hz, 2H), 8.31 (d, J = 8.8 Hz, 2H), 8.07 (d, J = 9.1 Hz, 2H), 7.95 (d, J = 8.0 Hz, 2H), 7.75 (d, J = 8.4 Hz, 2H), 7.68−7.62 (m, 4H), 7.03 (d, J = 9.2 Hz, 2H), 6.54 (s, 2H), 4.16 (d, J = 12.2 Hz, 2H), 3.91−3.83 (m, 4H), 2.99−2.95 (m, 2H), 2.90−2.84 (m, 2H), 2.52 (s, 2H), 2.48− 2.42 (m, 2H), 1.82 (t, 2H), 1.01−0.94 (m, 4H), 0.66 (d, J = 8.4 Hz, 2H), 0.56 (dd, J = 13.7, 7.1 Hz, 2H). ^{13}C NMR (151 MHz, CD$_3$CN) δ 171.20, 171.20, 151.26, 151.26, 148.39, 148.39, 146.11, 146.11, 140.07, 140.07, 139.77, 139.77, 136.24, 136.24, 131.76, 131.76, 129.42, 129.42, 128.14, 128.14, 126.65, 126.65, 125.96, 125.96, 124.33, 124.33, 123.25, 123.25, 117.66, 117.66, 72.50, 72.50, 67.81, 67.81, 43.47, 43.47, 28.87, 28.87, 24.25, 24.25.

[Ir(L2a)(en)](PF$_6$) (2a). Yield: 94%. Anal. Calcd. for C$_{44}$H$_{50}$F$_6$IrN$_4$O$_6$P: C 49.48, H 4.72, N 5.25. Found: C 49.34, H 5.18, N 5.55. HRMS Calcd. for [C$_{44}$H$_{50}$IrN$_4$O$_6$]$^+$, m/ z = 923.33541. Found: 923.33495 [M-PF$_6$]$^+$. ^{1}H NMR (600 MHz, CD$_3$CN) δ 8.51 (d, J = 8.8 Hz, 2H), 8.30 (d, J = 8.8 Hz, 2H), 8.08 (d, J = 8.6 Hz, 2H), 7.97 (d, J = 8.1 Hz, 2H), 7.78 (d, J = 8.3 Hz, 2H), 7.68−7.63 (m, 4H), 7.06 (d, J = 8.0 Hz, 2H), 6.62 (s, 2H), 4.24 (d, J = 11.8 Hz, 2H), 4.03 (d, J = 11.8 Hz, 2H), 3.87 (d, J = 12.4 Hz, 2H), 3.38−3.25 (m, 20H), 2.55 (s, 2H), 2.47 (s, 2H), 1.87 (t, 2H). ^{13}C NMR (151 MHz, CD$_3$CN) δ 171.28, 171.28, 150.63, 150.63, 148.30, 148.30, 145.95, 145.95, 140.16, 140.16, 139.75, 139.75, 134.68, 134.68, 131.71, 131.71, 129.41, 129.41, 128.26, 128.26, 126.66, 126.66, 126.37, 126.37, 124.56, 124.56, 121.87, 121.87, 117.72, 117.72, 72.48, 72.48, 70.15, 70.15, 70.13, 70.13, 70.10, 70.10, 70.00, 70.00, 69.50, 69.50, 43.44, 43.44.

[Ir(L2a)(men)](PF$_6$) (3a). Yield, 90%. Anal. Calcd. for C$_{45}$H$_{52}$F$_6$IrN$_4$O$_6$P: C 49.95, H 4.84, N 5.18. Found: C 50.16, H 4.64, N 5.39. HRMS Calcd. for [C$_{45}$H$_{52}$IrN$_4$O$_6$]$^+$, m/z = 937.35106. Found: 937.35034 [M-PF$_6$]$^+$. ^{1}H NMR (600 MHz, CD$_3$CN) δ 8.51 (d, J = 8.7 Hz, 2H), 8.33−8.29 (m, 2H), 8.10−8.07 (m, 2H), 8.00−7.94 (m, 2H), 7.83 (d, J = 8.3 Hz, 1H), 7.77 (d, J = 8.3 Hz, 1H), 7.70−7.64 (m, 4H), 7.09−7.03 (m, 2H), 6.61 (s, 1H), 6.55 (s, 1H), 4.28−4.21 (m, 2H), 4.07−3.98 (m, 3H), 3.86 (d, J = 11.7 Hz, 1H), 3.39−3.30 (m, 16H), 3.11−3.07 (m, 4H), 2.70−2.53 (m, 2H), 2.27 (d, J =

12.3 Hz, 2H), 1.73−1.52 (m, 1H), 0.85 (d, J = 6.1 Hz, 3H).^{13}C NMR (151 MHz, CD_3CN) δ 171.35, 171.27, 151.06, 150.59, 148.29, 148.19, 146.02, 145.92, 140.17, 139.98, 139.92, 139.84, 134.71, 134.51, 131.74, 131.61, 129.50, 129.47, 128.41, 128.31, 126.75, 126.69, 126.43, 126.31, 124.66, 124.44, 121.93, 121.89, 117.78, 117.75, 72.53, 72.52, 70.12, 70.12, 70.10, 70.10, 70.05, 70.05, 69.97, 69.97, 69.48, 69.48, 51.58, 48.90, 17.36.

[Ir(L4a)₂(en)](PF₆) **(4a)**. Yield: 98%. Anal. Calcd. for $C_{38}H_{40}F_6IrN_4O_2P$: C 49.51, H 4.37, N 6.08. Found: C 49.64, H 4.68, N 6.29. HRMS Calcd. for $[C_{38}H_{40}IrN_4O_2]^+$, m/z = 777.27750. Found: 777.27601 $[M-PF_6]^+$. ^{1}H NMR (600 MHz, CD_3CN) δ 8.50 (d, J = 8.3 Hz, 2H), 8.28 (d, J = 8.5 Hz, 2H), 8.07 (d, J = 6.6 Hz, 2H), 7.93 (d, J = 7.6 Hz, 2H), 7.81 (d, J = 7.5 Hz, 2H), 7.67 (s, 4H), 6.97 (d, J = 7.3 Hz, 2H), 6.62 (s, 2H), 4.10 (s, 4H), 3.97−3.84 (m, 2H), 3.15 (d, J = 30.9 Hz, 4H), 2.58 (s, 2H), 2.50 (s, 2H), 1.90 (s, 2H), 0.80 (s, 6H). ^{13}C NMR (151 MHz, CD_3CN) δ 171.27, 171.27, 150.50, 150.50, 148.30, 148.30, 145.80, 145.80, 140.61, 140.61, 139.81, 139.81, 134.18, 134.18, 131.79, 131.79, 129.41, 129.41, 128.29, 128.29, 126.69, 126.69, 126.34, 126.34, 124.69, 124.69, 121.44, 121.44, 117.63, 117.63, 71.66, 71.66, 64.96, 64.96, 43.48, 43.48, 14.27, 14.27.

General Procedure for the Synthesis of Macrocycle Complexes via In Situ C−N Coupling as a Locking Fragment. To synthesize a metallocycle complex, the diamine complex (0.05 mmol) was dispersed in 40 mL of ethanol within a 50-mL glass vessel equipped with an O_2 balloon. The solution was stirred at 60 °C and irradiated with an 80 W blue LED for 3 days. Upon removal of the solvent, the crude product underwent purification through silica gel column chromatography using a CH_2Cl_2/MeOH mixture (100/0 to 100/2 v/v) as the eluent, to isolate the desired macrocycle complex.

[Ir(L1)](PF₆) **(1)**. Yield, 90%. Anal. Calcd. for $C_{40}H_{38}F_6IrN_4O_2P$: C 50.90, H 4.06, N 5.94. Found: C 50.54, H 4.33, N 5.42. HRMS Calcd. for $[C_{40}H_{38}IrN_4O_2]^+$, m/z = 799.26295. Found: 799.26251 $[M-PF_6]^+$. ^{1}H NMR (600 MHz, CD_3CN) δ 8.50 (d, J = 9.0 Hz, 2H), 8.29 (d, J = 9.0 Hz, 2H), 8.11 (d, J = 9.0 Hz, 2H), 7.91 (d, J = 7.9 Hz, 2H), 7.87 (d, J = 7.3 Hz, 2H), 7.77−7.74 (m, 2H), 6.93 (d, J = 9.0 Hz, 2H), 6.48 (s, 2H), 5.81 (s, 2H), 4.27 (d, J = 12.2 Hz, 2H), 3.65 (d, J = 12.2 Hz, 2H), 3.32 (d, J = 10.2 Hz, 2H), 3.06−3.00 (m, 4H), 2.67−2.62 (m, 2H), 1.56 (s, 2H), 1.09 (s, 2H), 0.62−0.55 (m, 2H), 0.53−0.48 (m, 2H). ^{13}C NMR (151 MHz, CD_3CN) δ 163.58, 163.58, 147.73, 147.73, 146.17, 146.17, 145.13, 145.13, 143.44, 143.44, 140.36, 140.36, 135.52, 135.52, 132.59, 132.59, 129.45, 129.45, 128.57, 128.57, 128.05, 128.05, 126.29, 126.29, 122.91, 122.91, 118.33, 118.33, 72.30, 72.30, 66.74, 66.74, 53.63, 53.63, 28.82, 28.82, 26.62, 26.62, 23.86, 23.86.

[Ir(L2)](PF₆) **(2)**. Yield: 98%. Anal. Calcd. for $C_{44}H_{46}F_6IrN_4O_6P$: C 49.67, H 4.36, N 5.27. Found: C 49.44, H 4.78, N 5.39. HRMS Calcd. for $[C_{44}H_{46}IrN_4O_6]^+$, m/z = 919.30411. Found: 919.30286 $[M-PF_6]^+$. ^{1}H NMR (600 MHz, CD_3CN) δ 8.50 (d, J = 8.9 Hz, 2H), 8.28 (d, J = 9.0 Hz, 2H), 8.12 (d, J = 8.0 Hz, 2H), 7.93 (d, J = 8.0 Hz, 2H), 7.88−7.85 (m, 2H), 7.76 (t, 2H), 6.97 (d, J = 7.9 Hz, 2H), 6.45 (s, 2H), 5.90 (s, 2H), 4.22 (d, J = 12.0 Hz, 2H), 4.05 (d, J = 12.0 Hz, 2H), 3.50−3.30 (m, 20H), 3.18−3.12 (m, 2H), 3.02 (d, J = 11.0 Hz, 2H). ^{13}C NMR (151 MHz, CD_3CN) δ 163.48, 163.48, 147.63, 147.63, 146.10, 146.10, 145.32, 145.32, 143.42, 143.42, 140.57, 140.57, 135.46, 135.46, 130.47, 130.47, 129.53, 129.53, 128.63, 128.63, 128.27, 128.27, 128.07, 128.07, 126.57,

126.57, 121.29, 121.29, 118.42, 118.42, 72.40, 72.40, 70.18, 70.18, 70.15, 70.15, 70.12, 70.12, 69.95, 69.95, 69.47, 69.47, 53.74, 53.74.

[Ir(L3)](PF₆) **(3)**. Yield: 88%. Anal. Calcd. for $C_{45}H_{48}F_6IrN_4O_6P$: C 50.13, H 4.49, N 5.20; Found: C 49.89, H 4.76, N 5.42. HRMS Calcd. for $[C_{45}H_{48}IrN_4O_6]^+$, m/z = 933.31976. Found: 933.31946 $[M-PF_6]^+$. ^{1}H NMR (600 MHz, CD_3CN) δ 8.52−8.47 (m, 2H), 8.31−8.25 (m, 2H), 8.13−8.09 (m, 2H), 7.96−7.84 (m, 4H), 7.77−7.73 (m, 2H), 7.00−6.94 (m, 2H), 6.49 (s, 2H), 5.89 (s, 1H), 5.69 (s, 1H), 4.26−4.16 (m, 2H), 4.07−4.01 (m, 2H), 3.79−3.72 (m, 1H), 3.49−3.28 (m, 21H), 3.20−3.16 (m, 1H), 0.58 (d, J = 7.1 Hz, 3H). ^{13}C NMR (151 MHz, CD_3CN) δ 163.47, 163.32, 148.16, 146.88, 146.19, 145.83, 145.69, 145.11, 145.04, 144.54, 140.79, 140.72, 135.43, 135.38, 130.45, 129.80, 129.27, 128.97, 128.66, 128.60, 128.35, 128.29, 127.97, 127.88, 126.71, 126.51, 121.36, 121.32, 118.57, 118.37, 72.35, 72.35, 70.28, 70.28, 70.28, 70.28, 70.27, 70.27, 70.04, 70.04, 69.55, 69.48, 66.12, 58.80, 18.00.

[Ir(L4)](PF₆) **(4)**. Yield: 98%. Anal. Calcd. for $C_{38}H_{36}F_6IrN_4O_2P$: C 49.72, H 3.95, N 6.10. Found: C 49.50, H 3.47, N 6.36. HRMS Calcd. for $[C_{38}H_{36}IrN_4O_2]^+$, m/z = 773.24620. Found: 773.24546 $[M-PF_6]^+$. ^{1}H NMR (600 MHz, CD_3CN) δ 8.49 (d, J = 8.9 Hz, 2H), 8.26 (d, J = 9.0 Hz, 2H), 8.12 (d, J = 8.2 Hz, 2H), 7.90 (d, J = 7.9 Hz, 2H), 7.85 (d, J = 7.4 Hz, 2H), 7.76 (t, 2H), 6.89 (d, J = 7.8 Hz, 2H), 6.46 (s, 2H), 5.90 (s, 2H), 4.10 (d, J = 4.3 Hz, 4H), 3.30 (d, J = 9.8 Hz, 2H), 3.24 (d, J = 7.0 Hz, 4H), 3.01 (d, J = 10.6 Hz, 2H), 0.94 (t, 6H). ^{13}C NMR (151 MHz, CD_3CN) δ 163.42, 163.42, 147.77, 147.77, 146.10, 146.10, 145.24, 145.24, 143.42, 143.42, 141.01, 141.01, 135.40, 135.40, 130.08, 130.08, 129.57, 129.57, 128.63, 128.63, 128.28, 128.28, 128.04, 128.04, 126.47, 126.47, 120.93, 120.93, 118.41, 118.41, 71.73, 71.73, 65.32, 65.32, 53.77, 53.77, 14.33, 14.33.

General Procedure for Photooxidation of Sulfide into Sulfoxide. For the transformation of sulfide into sulfoxide, the sulfide (0.1 mmol) and photocatalyst (1 mol %) were dispersed in 20 mL of distilled water within a 25-mL quartz tube, which was outfitted with an O_2 balloon. The reaction mixture was subjected to irradiation from an 80 W blue LED at ambient temperature for 12 h. The reaction mixture was then extracted using CH_2Cl_2 three times (3 × 15 mL). The CH_2Cl_2 layer was collected, sequentially washed with water and brine, and dried over anhydrous Na_2SO_4. The organic layer was then concentrated for NMR analysis. To further purify the product, the crude product underwent silica gel column chromatography, employing a hexane/ethyl acetate (10:1, V/V) mixture as the eluent to yield the desired sulfoxide.

■ RESULTS AND DISCUSSION

Synthesis and Structural Characterization of Ir(III) Macrocycle Complexes. Metal-template synthesis plays an important role in macrocycle and supramolecular chemistry. A prototypical instance is the synthesis of tetraaza macrocycle 1,4,8,11-tetraazacyclotetradecane (cyclam), which is typically synthesized via Schiff base condensation of glyoxal with a long chain tetraamine, using Ni(II) as a template. This process yields high product concentrations under benign conditions and is followed by hydrogenation by $NaBH_4$, as depicted in Scheme 2.[17] Inspired by this seminal work, we aimed to establish a new methodology for the synthesis of cyclo-metalated macrocycle complexes. This new approach is based on our previously developed protocol for the amination of the

Scheme 2. Template Synthesis of Macrocycle Complexes
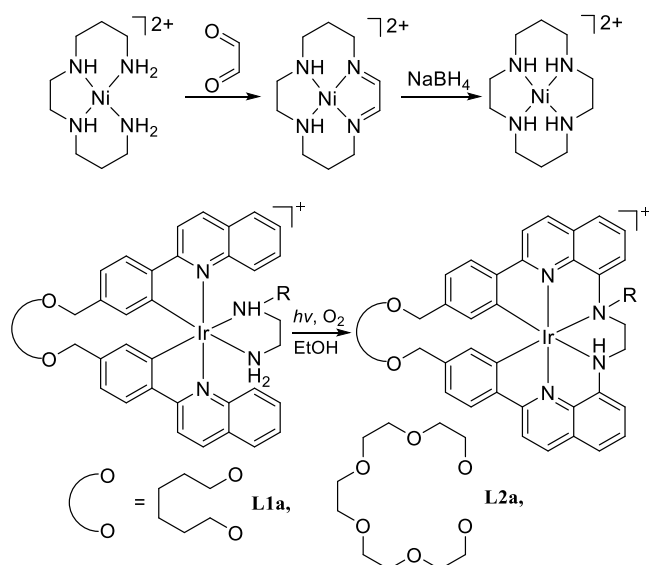
coordinated pq complexes through in situ interligand C−N cross-coupling under visible light irradiation,[14,15] serving as a locking fragment, as illustrated in Scheme 2. Consequently, we designed and synthesized C-shape ligands **L1a** and **L2a**, which bridge two symmetric pq arms via a flexible chain, for further cyclization with diamine in the presence of a metal ion as a template under mild conditions (for further details, see the Supporting Information).

The synthesis of ligand **L1a** started with the reaction of long-chain diols and *p*-bromobenzyl bromide in the presence of NaH in THF solution, according to the reported procedures.[18] This reaction achieved a high yield of 90%, as shown in Scheme 3. Subsequently, a two-step Miyaura−Suzuki reaction

Scheme 3. Summary of the Synthesis of Macrocycle Complexes
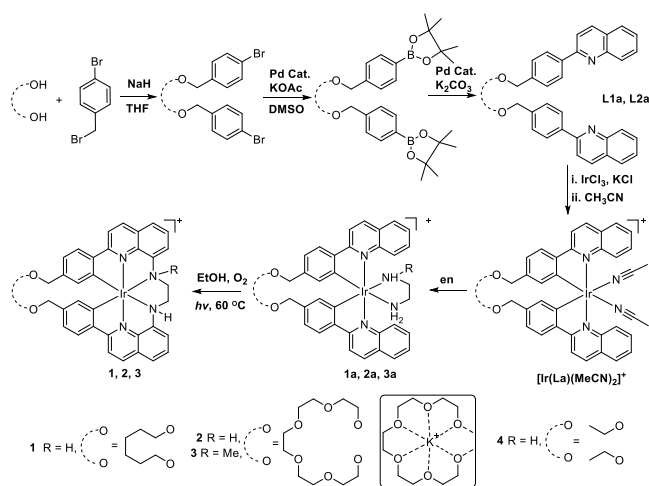
involving bis(pinacolato)diboron and 2-bromoquinline, in the presence of Pd catalysts, yielded the long chain linked bis-pq ligand **L1a** with an isolated yield of 84%.[19] The base peak in the HRMS analysis (m/z = 553.28476) corresponded to the $[M + H]^+$ ion. Both ^1H and ^{13}C NMR spectra corroborated the symmetrical structure of **L1a**, as illustrated in Scheme 3.

Subsequently, ligand **L1a** was used to synthesize dimeric complex $[Ir_2(\textbf{L1a})_2(\mu\text{-Cl})_2]$ to ensure that the two pq sites from a single **L1a** ligand underwent cyclometalation at one Ir(III) center, according to the published procedure.[20] Indeed, treatment of 2-methoxyethanol suspensions of iridium(III) trichloride with 1.25 equiv of **L1a** ligand at 120 °C for 24 h produced a precipitation of the dimer $[Ir_2(\textbf{L1a})_2(\mu\text{-Cl})_2]$ as a pale red solid, which was sequentially converted into the high reactive mononuclear precursor $[Ir(\textbf{L1a})(MeCN)_2](PF_6)$ by treatment with MeCN at 80 °C. Its structure and composition were confirmed by HRMS and NMR spectroscopy. As expected, the $[Ir(\textbf{L1a})(MeCN)_2](PF_6)$ complex exhibited a symmetrical fashion in NMR spectra. However, in contrast to previous studies on nonchain bidentate ligands such as ppy and pq-Ir(III) complexes,[20] the synthesis yield of $[Ir(\textbf{L1a})\text{-}(MeCN)_2](PF_6)$ was comparatively lower at 35%, akin to that of complex B at 33.4% (refer to Scheme 1).[6b] This reduced yield can be attributed to the flexible nature of the two pq arms in the **L1a** ligand, which is spatially distant and exhibits significant thermodynamic oscillation that is not conducive to the formation of mononuclear complexes.[6c,21]

To address the issue of low yield, ligand **L2a**, featuring an 18-crown-6 ether scaffold, was designed and synthesized with a high yield following the same procedure as **L1a** (see the Supporting Information for details). We hypothesized that the template effect of the 18-crown-6 ether-like in conjunction with the K$^+$ cation would effectively draw the pq groups of the two arms into closer proximity,[22] facilitating the coordination of both pq arms from a single **L2a** ligand to one Ir(III) center, thus leading to the formation of the dimeric $[Ir_2(\textbf{L2a})_2(\mu\text{-Cl})_2]$ complex. This dimeric precursor was then transformed into the mononuclear $[Ir(\textbf{L2a})(MeCN)_2](PF_6)$ complex. Remarkably, the addition of 2 equiv. of KCl to the **L2a** reaction solution at 120 °C increased the yield of $[Ir(\textbf{L2a})\text{-}(MeCN)_2](PF_6)$ from 30% to 85% and reduced the reaction time to 6 h, suggesting a substantial enhancement in the formation of the dimeric precursor due to the K$^+$ ion. Conversely, the addition of KCl to the **L1a** reaction solution did not exhibit a significant effect on the synthesis of $[Ir(\textbf{L1a})(MeCN)_2](PF_6)$ complex. The influence of the Na$^+$ cation as a template was also explored; replacing KCl with NaCl under identical conditions increased the reaction yield to 60%, though this was less effective than the 85% yield achieved with K$^+$. Moreover, altering the linker position from the para-phenyl to the meta-phenyl on the pq ligand did not yield the desired dimeric Ir(III) complex under the same synthetic conditions, indicating the crucial role of the pq arm connection site in forming the C-shape Ir(III) complex. To further investigate the template effect of the K$^+$ cation, MS and fluorescence techniques were employed. Early in the reaction, HRMS analysis of the reaction solution identified a prominent peak at m/z = 711.28204 (see Figure S1 in the Supporting Information), aligning with the calculated isotope pattern for $[\textbf{L2a}+K]^+$ (m/z = 711.28310), confirming the formation of the $[K\textbf{L2a}]$ complex. Additionally, an increase in fluorescence emission of **L2a** in the presence of K$^+$ ion was observed (see Figure S1 in the Supporting Information), attributable to the augmented rigidity of the **L2a** ligand upon K$^+$ ion binding.[23] These findings elucidate that the K$^+$ ion initially coordinates to the 18 crown-6 ether segment of the **L2a** ligand, positioning the pq arms suitably for chelation to an Ir(III) ion and facilitating the dimeric $[Ir_2(\textbf{L2a})_2(\mu\text{-Cl})_2]$ complex formation. Therefore, employing a polyether chain as a template with a K$^+$

ion emerges as a viable and effective strategy for synthesizing tetradentate C^O long-chain linked cyclometal Ir(III) complexes.

With the highly reactive precursor at our disposal, a suite of diamine Ir(III) complexes **1a−4a** were synthesized by the reaction of $[Ir(La)(MeCN)_2]PF_6$ with the corresponding diamine ligand under mild conditions, achieving nearly quantitative yield, as shown in Scheme 3. The structural integrity and compositional accuracy of these complexes were validated by elemental analysis, NMR, and HRMS spectrometry, with detailed data available in the experimental section and Supporting Information. The ^1H NMR spectra of the coordinated en displayed two sect of resonance peaks around 3.87 and 2.55 ppm (attributed to the NH_2 group) and another two sets around 2.47 and 1.87 ppm (assigned to the CH_2 group). Additionally, the ^{13}C NMR spectra revealed resonance peaks at 43.47, 43.44, 48.90, and 51.58, and 43.48 ppm for complexes **1a**, **2a**, **3a**, and **4a**, respectively. These findings are in agreement with previous observations reported for [Ir-(pq)_2(en)](PF_6) complex.[15]

To further substantiate the structural configuration, the single-crystal structure of **1a** was determined by X-ray diffraction (see Table S1). The complex crystallized in the $P2_1/c$ space group. As anticipated, the Ir(III) ion in each molecule is coordinated by an en ligand and two pq units from an **L1a** ligand, adopting a distorted octahedral geometry, as illustrated in Figure 1. Notably, the Ir−N bond lengths in the
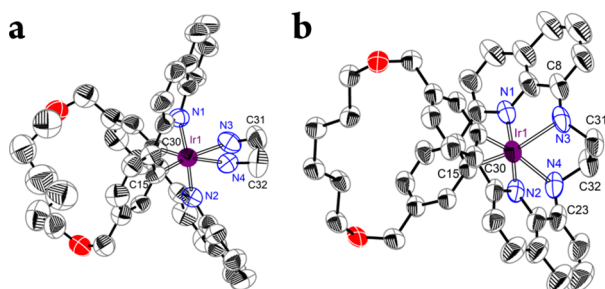

Figure 1. Crystal structures of **1a** (a) and **1** (b) with 50% probability of ellipsoids. H atoms and anion are omitted for clarity. Selected bond lengths (Å) and angles (deg) for **1a** and **1** (in parentheses): Ir1−N1 = 2.068(10) (1.951(10)), Ir1−N2 = 2.080(11) (1.951(10)), Ir1−N3 = 2.233(10) (2.218(7)), Ir1−N4 = 2.237(20) (2.218(7)), Ir1−C15 = 1.980(11) (2.012(8)), Ir1−C30 = 2.015(13) (2.012(8)), C31−N3= 1.472(16) (1.521(12)), C32−N4= 1.452(15) (1.521(12)), N3−C8 = (1.492(15)), N4−C23 = (1.492(15)); ∠N3−Ir1−N4 = 75.5(4) (80.2(4)), ∠N1−Ir1−N2 = 173.5(4) (176.4(4)).

en ligand (2.233(10) and 2.237(10) Å) are significantly elongated compared with those in the pq units (2.068(10) and 2.080(11) Å), a phenomenon likely stemming from the trans effect of the Ir−C bond. The two symmetric pq units are interconnected by a long chain featuring C−O and C−C single bonds. Each **L1a** ligand anchors to an Ir(III) ion in a C-shape conformation, with the quinoline arms positioned trans to each other, denoted by a bond angle of N1−Ir1−N2 at 173.5(4)°. Other details align with those reported in previous studies.[15]

The cyclization of $[Ir(La)(en)](PF_6)$ complexes was conducted leveraging our previously developed in situ interligand C−N cross-coupling under visible light irradiation,[14,15] as depicted in Scheme 3. Complex **1a** served as a prototype to refine the photoreaction conditions and analyze spectral changes. When an ethanol solution of **1a** was

irradiated with visible light at 60 °C for 3 days in an oxygen-rich atmosphere, new C−N coupling macrocyclic product **1** was obtained in an excellent yield of 90% after purification. HRMS analysis of **1** revealed a molecular ion peak at m/z 799.26251, consistent with the theoretical isotope pattern for $C_{40}H_{38}IrN_4O_2$ (m/z = 799.26295, $[M-PF_6]^+$), which is four units less than that of **1a** (m/z = 803.29425, $[M-PF_6]^+$), indicative of the loss of four hydrogen atoms and the formation of two C−N bonds during the photoreaction. A comparative analysis of the ^1H NMR spectra between **1a** and **1** revealed the disappearance of the characteristic resonance peak of H8 of the quinoline ring at 7.75 ppm in **1a**. As illustrated in Figure 2, the
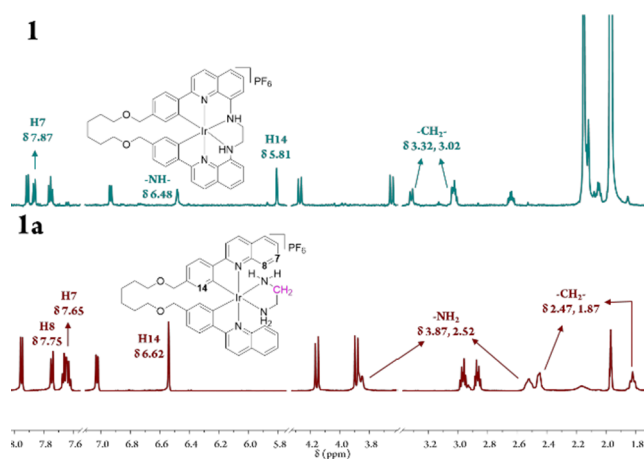

Figure 2. ^1H NMR spectra of complexes **1** and **1a** in CD_3CN.

resonances of the NH_2 (3.87 and 2.52 ppm) and the CH_2 (2.74 and 1.87 ppm) groups of the en ligand in **1a** shifted to 6.45 and 3.31 and 3.02 ppm in **1**, respectively. The ^{13}C NMR spectra of **1** displayed a shift in the characteristic peak of the en ligand from 43.47 to 53.74 ppm (refer to the Supporting Information). These results collectively suggest that the en ligand in **1a** underwent in situ C−N cross-coupling with the pq units of the **L1a** ligand under visible light irradiation, resulting in the formation of macrocycle ligand **L1**. Notably, this method represents the inaugural instance of employing in situ C−N cross-coupling for the synthesis of cyclometalated macrocycle complexes. Additionally, this cyclization protocol was successfully replicated to synthesize cyclometalated macrocycle complexes **2** and **3**, using **2a** and **3a** as substrates, under identical conditions in excellent yields of 98 and 88%, respectively. The structural integrity and compositional accuracy of these complexes were corroborated by elemental analysis, HRMS, and NMR spectroscopy. This strategy offers a feasible and rational protocol for the synthesis of cyclometalated macrocycle Ir(III) complexes via in situ postcoordinated interligand C−N cross-coupling reaction under benign conditions, resulting in exceptional yields.

To further confirm the structure of the cyclometalated macrocycle complex, the single-crystal structure of **1** was elucidated by X-ray diffraction, with details provided in Table S1 in the Supporting Information. The complex crystallized in the $P4/nnc$ space group, exhibiting higher symmetry compared to that of **1a** in the $P2_1/c$. In line with expectations, two new C8−N3 (1.492(15) Å) and C23−N4 (1.492(15) Å) bonds were indeed formed through interligand C−N coupling between the two pq units and the en ligand, resulting in the formation of new macrocycle ligand **L1**. The Ir(III) ion in **1** is

Table 1. Photophysical Data for Complexes 1−4, 2a, and 4a[a]

complex	λ_{abs} (nm) (ε[$\times 10^3$ M^{-1} cm^{-1}])	λ_{em} (nm)	τ_1 (ns)[b]	τ_2 (ns)[b]	Φ (%)[c]	k_r ($\times 10^5$ s^{-1})[d]	k_{nr} ($\times 10^5$ s^{-1})[d]	Φ_Δ[e]
1a	272 (30.1), 342 (14.6), 456 (3.1)	583	392.3	320.1	27.4	8.6	22.7	32.1
1	263 (21.4), 348 (6.8), 457 (2.1)	591, 635 (sh)	873.2	285.9	16.5	1.9	9.6	54.4
2a	265 (29.5), 339 (12.9), 457 (2.3)	594	674.5	161.0	17.7	2.6	12.2	24.1
2	263 (19.7), 348 (6.1), 457 (2.2)	593, 635 (sh)	917.4	207.5	16.5	1.8	9.1	53.1
3	272 (20.1), 348 (8.1), 457 (2.8)	592, 633 (sh)	1080.1	251.5	14.1	1.3	7.9	56.7
4a	272 (32.2), 341 (15.5), 456 (3.1)	596	385.3	150.8	29.0	7.5	18.4	28.5
4	271 (25.7), 348 (10.6), 457 (3.5)	589, 632 (sh)	924.8	217.8	9.2	1.0	9.8	49.5

[a]All photophysical data were measured in the methanol solvent at room temperature. [b]Excitation at 405 nm. τ_1 is the fluorescence lifetime in N$_2$-saturated methanol, and τ_2 is the fluorescence lifetime in O$_2$-saturated methanol. [c]Excitation at 347 nm. ϕ is the quantum yield in Ar-saturated methanol. [d]Calculated according to the equations $k_r = \Phi/\tau_1$ and $k_{nr} = (1 - \Phi)/\tau_1$, where k_r is the radiative rate constant, k_{nr} is the nonradiative rate constant. [e]Φ_Δ is the ^{1}O$_2$ generation quantum yield in air-saturated methanol.

coordinated by two carbons and four nitrogens from a hexadentate macrocycle ligand **L1**, assuming a distorted octahedral geometry, as depicted in Figure 1. A structural comparison between **1** and **1a** reveals enlargement in the bite angle of N3−Ir1−N4 in **1** to 80.2(4)°, up from 75.5(4)° in **1a**, with other parameters showing similarity.

Photophysical Properties of Cyclometalated Macrocycle Ir(III) Complexes. The UV−vis absorption spectra of the cyclometalated macrocyle Ir(III) complexes **1**, **2**, and **3**, as well as the acyclic counterparts **1a**, **2a**, **4a**, and **4**, were acquired in MeOH solutions and are detailed in Table 1 and Figure S2. In accordance with previous studies on related Ir(III)−pq complexes,[24] the intense absorption bands observed at 263−272 nm in these complexes are attributable to spin-allowed $\pi-\pi^*$ ligand-centered (LC) transitions within the pq segments. Additionally, the moderately intense band occurring at 339−348 nm is ascribed to spin-allowed metal-to-ligand charge transfer (^{1}MLCT), while the less pronounced band around 457 nm is primarily due to spin-forbidden ^{3}MLCT transitions. Notably, there is no significant difference in the absorption characteristics between the macrocyclic Ir(III)−pq complexes and their acyclic equivalents.

The emission spectra and lifetimes as well as quantum yields of the complexes were measured in MeOH solution at room temperature and are summarized in Table 1 and Figures S3−S8. Complexes show an orange-red emission with a maximum emission band at about 590 nm and a shoulder at 632 nm, which can be assigned to a ^{3}LC ($\pi-\pi^*$) and ^{3}MLCT transitions.[24] The emission wavelengths had no noticeable change between the cyclic and acyclic complexes, but the lifetime significantly increased from 392 ns for **1a**, 674 ns for **2a**, and 385 ns for **4a** to 873 ns for **1**, 917 ns for **2**, 1080 ns for **3**, and 924 ns for **4** in N$_2$-saturated methanol solution. This can be attributed to the robust rigidity of the macrocycle complexes.

For comparative analysis, the emission spectra and lifetimes of the complexes were also recorded in an O$_2$-saturated MeOH solution at room temperature. In O$_2$-saturated MeOH, a decrease in emission intensity was observed, and the lifetimes were reduced to 320 ns for **1a**, 285 ns for **1**, 161 ns for **2a**, 207 ns for **2**, 251 ns for **3**, 150 ns for **4a**, and 217 ns for **4**. These results, presented in Figure 3 and the Supporting Information, suggest that these complexes are susceptible to O$_2$ quenching. The quantum yields of the cyclometalated complexes were quantified as ranging from 9.2% to 29% using an absolute measurement method with an integrating sphere in Ar-saturated methanol at room temperature.
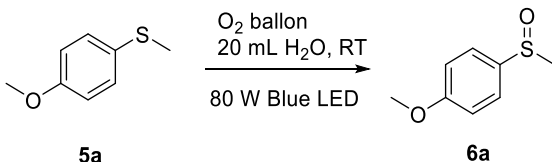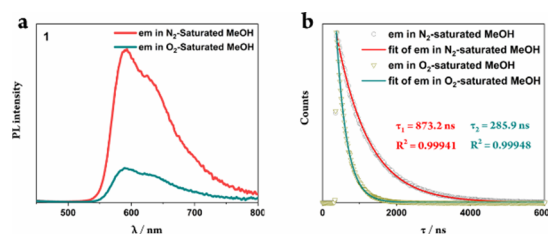

Figure 3. (a) PL spectra of **1** in N$_2$-saturated (red) and O$_2$-saturated (dark cyan) MeOH at room temperature. (b) Single-wavelength decay traces for **1** in N$_2$-saturated (red) and O$_2$-saturated (dark cyan) MeOH at room temperature.

The experimental results demonstrate that these Ir(III) complexes exhibit sensitivity to O$_2$ and maintain structural integrity under light irradiation, suggesting their potential as effective photosensitizers and photocatalysts for photoreaction. Consequently, we evaluated the efficiency of ^{1}O$_2$ generation (Φ_Δ), a primary reactive oxygen species (ROS) in photoreaction under O$_2$ atmosphere. Φ_Δ is correlated with the triplet excited state energy, lifetime, and quantum yield and was determined in air-saturated MeOH using Rose Bengal as a reference and DPBF as a trapping agent, as detailed in Figure S9 in the Supporting Information.[25] Table 1 illustrates that the Φ_Δ values for the cyclometalated macrocycle complexes **1** (54%), **2** (53%), and **3** (56%) are substantially higher than those of the acyclic complexes **1a** (32%) and **2a** (24%). Notably, the Φ_Δ for the tetradentate Ir(III) complex **4** (49%) shows a marked increase compared to the bidentate Ir(III) complex **4a** (28%). These findings indicate that the cyclometalated macrocycle compounds possess stable and efficient singlet oxygen generation abilities under blue light radiation and exhibit significant distinctions from cage Ir(III) complexes (where the metal ion is enveloped and shielded from O$_2$ quenchers),[8] thereby underscoring that the ligand topology profoundly influences the photophysical and photochemical properties of cyclometalated Ir(III) complexes.

Photo-Oxidation of Sulfide into Sulfoxide. Sulfoxides, integral in organic synthesis and the pharmaceutical industry,[26] have garnered significant interest for aerobic photo-oxidation of sulfides, viewed as a straightforward and eco-friendly route utilizing visible light as an energy source and oxygen as an oxidant.[27] However, challenges persist in sustainability and efficiency, primarily due to the degradation of photosensitizers under light irradiation. Thus, the development of a robust photosensitizer is essential. Additionally, water is an ideal green solvent,[28] yet catalytic oxidation of sulfide into sulfoxide in aqueous media remains challenging because of poor catalyst

solubility and sulfide incompatibility.[29] Inspired by the outstanding stability and efficient $^1O_2$ generation of cyclometalated Ir(III) complexes, we explored their photocatalytic reactivity in oxidizing sulfide into sulfoxide.[30] Methyl 4-methoxyphenyl sulfide (**5a**) was chosen as a model substrate to optimize reaction conditions using the synthesized Ir(III) complexes (1 mol %) as photocatalysts in an O_2 atmosphere in water under blue light irradiation at room temperature for 12 h. Gratifyingly, the photocatalytic reactions proceeded smoothly, yielding methyl 4-methoxyphenyl sulfoxide (**6a**) in excellent yields of 98%, 100%, and 96% with cyclometalated macrocycle Ir(III) complexes **1**, **2**, and **3** as catalysts, respectively (refer to entries 1−3 in Table 2). Furthermore,

Table 2. Photo-Oxidation of Sulfides[a]

entry	catalyst	DFSC[b]	yield (%)[c]
1	**1**		98
2	**2**		100
3	**3**		96
4	**4**		92
5	**1a**		86
6	**2a**		88
7	**4a**		66
8			0
9	**2**	N_2	0
10	**2**	dark	0
11	**2**	2 eq. G-SH	15
12	**2**	2 eq. DABCO	24
13	**2**	2 eq. ^{i}PrOH	99
14	**2**	2 eq. BQ	96
15	**2**	2 eq. DMB	98

[a]Reaction conditions: **5a** (0.1 mmol) and catalyst (1 mol %) in 20 mL H_2O with an O_2 balloon under an 80 W blue LED at RT for 12 h. [b]DFSC is the deviation from standard conditions. [c]Determined by ^{1}H NMR. G-SH is glutathione; DABCO is diazabicyclo[2.2.2]octane; BQ is benzoquinone; DMB is 1,4-dimethoxybenzene.

the photocatalytic reactions exhibited high chemoselectivity with no detectable byproducts. For comparative purpose, acyclic Ir(III) complexes **1a**, **2a**, **4**, and **4a** were also tested under identical conditions (see entries 4−7 in Table 2), yielding **6a** from 66% to 92%, albeit slightly lower than the macrocyclic counterparts. This is in line with the enhanced $^1O_2$ generation by the cyclometalated macrocycle Ir(III) complexes. Additionally, the recyclability of photocatalyst **2** was assessed by using **5a** as a model substrate under the same conditions. Postreaction, the reaction mixture was extracted by toluene three times (3 × 10 mL) to remove the product sulfoxide and unreacted substrate sulfide, followed by extraction of the aqueous layer with CH_2Cl_2 three times (3 × 10 mL). The recovered catalyst **2** was then reused in subsequent cycles, maintaining its catalytic efficiency for at least 10 cycles without significant activity loss, as depicted in Figure S65. The ^{1}H NMR spectra of recovered **2** showed that its structure was still maintained after 10 cycle reactions (see Figure S65b in the Supporting Information). These findings

underscore the long-term stability and exceptional photocatalytic prowess of the macrocycle Ir(III) complexes.

To gain insight into the photocatalytic reaction mechanism, control experiments were performed using **5a** as a model under identical conditions. Initially, these experiments confirmed that the photocatalyst, light, and oxygen are indispensable for the oxidation of sulfide into sulfoxide (see entries 8−10 in Table 2). Consequently, identifying the ROS involved in the photocatalytic process became paramount. Typically, two types of ROS intermediates such as $^1O_2$ and $O_2 \cdot^-$ have been proposed in photocatalytic oxidation processes in the presence of O_2.[31] To probe this, 2 equiv of inhibitors 1,4-diazabicyclo[2.2.2]octane (DABCO) and glutathione (G-SH) were introduced into the reaction mixture as scavengers of $^1O_2$. A notable reduction in the reaction yield to 15% and 24%, respectively (see entries 11 and 12 in Table 2), indicated the pivotal role of $^1O_2$. In contrast, the addition of 2 equiv. of benzoquinone (BQ), isopropyl alcohol (^{i}PrOH), and 1,4-dimethoxybenzene (DMB) as scavengers for superoxide radical, ·OH, and sulfide radical cation, respectively, had negligible impact on sulfoxide formation. These results strongly suggest $^1O_2$ as the primary ROS in the photo-oxidation process. Based on these observations, a reaction mechanism for sulfide photo-oxidation involving $^1O_2$ is proposed in Scheme 4: under blue light irradiation, the Ir(III)

Scheme 4. Proposed Mechanism of Photo-Oxidation of Sulfides
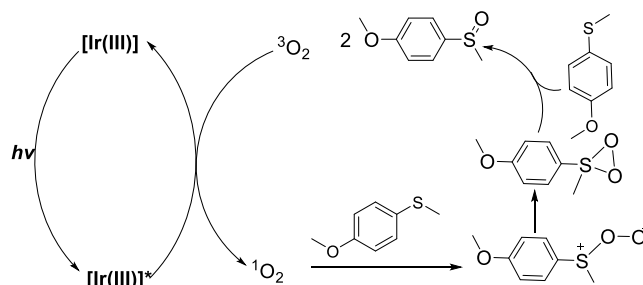
complex transitions to a high-energy excited singlet state ^{1}Ir(III)*, which rapidly undergoes intersystem crossing to a triplet ^{3}Ir(III)*, facilitated by efficient spin−orbit coupling in the Ir(III) complex. The ^{3}Ir(III)* then transfers energy to the ground-state $^3O_2$ to generate $^1O_2$. The $^1O_2$ thus reacts with sulfide to create a peroxy-sulfoxide intermediate, which immediately rearranges to a 3-membered ring thiadioxirane intermediate. The thiadioxirane intermediate facilely reacts with another sulfide molecule to yield two sulfoxide molecules.[32]

With optimal conditions established, we explored the broader applicability of our protocol for aerobic photo-oxidation of sulfide into sulfoxide. Initially, methylphenyl sulfide and aromatic sulfides with a para-methyl group were utilized as substrates in place of **5a**, under identical conditions. To our delight, the corresponding sulfoxide products **6b** and **6c** were efficiently synthesized, yielding isolated results of 98% in 8 h and 96% in 10 h, respectively, as presented in Table 3. Substituting methoxyphenyl with naphthyl gave a yield of 75% for **6d** over 3 days. Further, substitutions with an electron-withdrawing cyano group at *para* and Cl at *ortho* positions led to significantly reduced yields of the corresponding sulfoxides **6d** and **6f**, at 40% in 10 days and 58% in 15d, respectively. This

Table 3. Scope of the Photooxidation of Sulfides
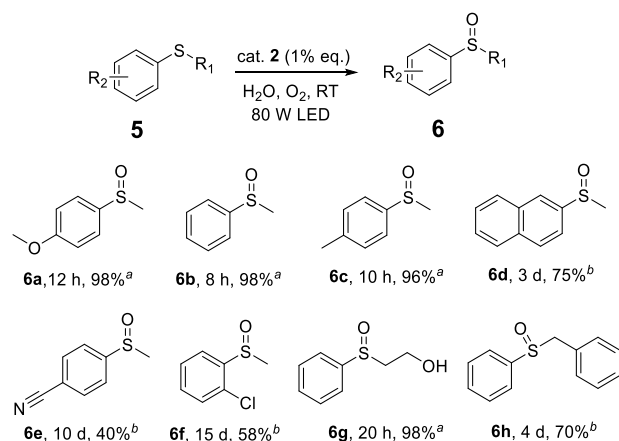
aIsolated yield. bDetermined by ^{1}H NMR.

suggests that electron-withdrawing group on the phenyl ring can effectively inhibit sulfide oxidation. Steris effects were also observed with substituted phenyl sulfide using 2-(phenylthio)-ethanol in place of methyl sulfide yielded sulfoxide **6g** with 98% efficiency over 20 h. Conversely, replacing methyl sulfide in **5a** with a benzyl group slowed the reaction, resulting in 70% of **6h** over 4 d. These experiments underscore the potential of this approach for synthesizing sulfoxide compounds via a green pathway.

CONCLUSIONS

In summary, we have successfully developed a mild and efficient protocol for synthesizing cyclometalated macrocycle Ir(III) complexes. This approach involves the preassembly of two symmetric pq arms into C-shaped complexes followed by cyclization with diamine via in situ interligand C−N cross-coupling, utilizing a metal ion as a template. This strategy offers a new and complementary protocol for in situ synthesis of metal macrocycle complexes employing a postcoordinated interligand-coupling approach under mild conditions. More-over, our research demonstrated that the use of 18-crown-6 ether scaffold in conjunction with K$^+$ ions is a viable and effective method for constructing C^O chain-linked cyclo-metalated Ir(III) complexes. We have also discovered that the ligand topology significantly influences the photophysical and photochemical properties of cyclometalated Ir(III) complexes. Notably, the macrocycle Ir(III) complexes exhibit exceptional stability and proficient singlet oxygen generation under blue light radiation. The synthesized cyclometalated macrocycle Ir(III) complexes displayed high photocatalytic activity and chemoselectivity in the aerobic oxidation of sulfide into sulfoxide in water at room temperature. These insights pave the way for an innovative strategy in designing and synthesizing macrocycle Ir(III) complexes as efficient photo-catalysts. The photocatalytic reactions using the synthesized macrocycle complexes as catalysts in aqueous media are currently underway in our group.

ASSOCIATED CONTENT

⑤ Supporting Information

The Supporting Information is available free of charge at https://pubs.acs.org/doi/10.1021/acsomega.4c01111.

General procedure for the synthesis of ligands **L1a** and **L2a**; crystallographic data for **1a** and **1**; photophysical spectra, NMR, and HRMS spectra of the complexes; recovery and photooxidation cycle of photocatalyst **2** (PDF)

■ AUTHOR INFORMATION

Corresponding Authors

Hai-Yun Zhou − *Instrumental Analysis and Research Center, Sun Yat-sen University, Guangzhou, Guangdong 510275, China*; Email: zhouhy@mail.sysu.edu.cn

Bao-Hui Ye − *MOE Key Laboratory of Bioinorganic and Synthetic Chemistry, School of Chemistry, Sun Yat-sen University, Guangzhou, Guangdong 510275, China*; ⓘ orcid.org/0000-0003-0990-6661; Email: cesybh@mail.sysu.edu.cn

Authors

Xiao-Kang Huang − *MOE Key Laboratory of Bioinorganic and Synthetic Chemistry, School of Chemistry, Sun Yat-sen University, Guangzhou, Guangdong 510275, China*

Gao-Feng Liu − *MOE Key Laboratory of Bioinorganic and Synthetic Chemistry, School of Chemistry, Sun Yat-sen University, Guangzhou, Guangdong 510275, China*; ⓘ orcid.org/0000-0002-7989-9017

Complete contact information is available at: https://pubs.acs.org/10.1021/acsomega.4c01111

Notes

The authors declare no competing financial interest.

■ REFERENCES

(1) (a) Chi, Y.; Chou, P.-T. Transition metal phosphors with cyclometalating ligands: fundamentals and applications. *Chem. Soc. Rev.* **2010**, *39*, 638−655. (b) Yersin, H.; Rausch, A. F.; Czerwieniec, R.; Hofbeck, T.; Fischer, T. The triplet state of organo-transition metal compounds. Triplet harvesting and singlet harvesting for efficient OLEDs. *Coord. Chem. Rev.* **2011**, *255*, 2622−2652. (c) You, Y.; Nam, W. Photofunctional triplet excited states of cyclometalated Ir(iii) complexes: beyond electroluminescence. *Chem. Soc. Rev.* **2012**, *41*, 7061−7084.

(2) (a) Lee, L. C.-C.; Lo, K. K.-W. Luminescent and Photofunc-tional Transition Metal Complexes: From Molecular Design to Diagnostic and Therapeutic Applications. *J. Am. Chem. Soc.* **2022**, *144*, 14420−14440. (b) Bi, X.-D.; Yang, R.; Zhou, Y.-C.; Chen, D.; Li, G.-K.; Guo, Y.-X.; Wang, M.-F.; Liu, D.; Gao, F. Cyclometalated Iridium(III) Complexes as High-Sensitivity Two-Photon Excited Mitochondria Dyes and Near-Infrared Photodynamic Therapy Agents. *Inorg. Chem.* **2020**, *59*, 14920−14931. (c) Wang, M.-F.; Yang, R.; Tang, S.-J.; Deng, Y.-A.; Li, G.-K.; Zhang, D.; Chen, D.; Ren, X.; Gao, F. In vivo Realization of Dual Photodynamic and

Photothermal Therapy for Melanoma by Mitochondria Targeting Dinuclear Ruthenium Complexes under Civil Infrared Low-power Laser. *Angew. Chem., Int. Ed.* **2022**, *61*, No. e202208721.

(3) Prier, C. K.; Rankic, D. A.; MacMillan, D. W. C. Visible Light Photoredox Catalysis with Transition Metal Complexes: Applications in Organic Synthesis. *Chem. Rev.* **2013**, *113*, 5322−5363.

(4) Albrecht, M. Cyclometalation Using d-Block Transition Metals: Fundamental Aspects and Recent Trends. *Chem. Rev.* **2010**, *110*, 576−623.

(5) (a) Gorczyński, A.; Harrowfield, J. M.; Patroniak, V.; Stefankiewicz, A. R. Quaterpyridines as Scaffolds for Functional Metallosupramolecular Materials. *Chem. Rev.* **2016**, *116*, 14620−14674. (b) Chi, Y.; Chang, T.-K.; Ganesan, P.; Rajakannu, P. Emissive bis-tridentate Ir(III) metal complexes: Tactics, photophysics and applications. *Coord. Chem. Rev.* **2017**, *346*, 91−100.

(6) (a) Lee, Y. H.; Park, J.; Lee, J.; Lee, S. U.; Lee, M. H. Impact of Restricted Rotation of o-Carborane on Phosphorescence Efficiency. *J. Am. Chem. Soc.* **2015**, *137*, 8018−8021. (b) Bünzli, A. M.; Pertegás, A.; Momblona, C.; Junquera-Hernández, J. M.; Constable, E. C.; Bolink, H. J.; Ortí, E.; Housecroft, C. E. [Ir(C^N)2 (N^N)]+ emitters containing a naphthalene unit within a linker between the two cyclometallating ligands. *Dalton Trans.* **2016**, *45*, 16379−16392. (c) Esteruelas, M. A.; López, A. M.; Oñate, E.; San-Torcuato, A.; Tsai, J.-Y.; Xia, C. Preparation of Phosphorescent Iridium(III) Complexes with a Dianionic C,C,C,C-Tetradentate Ligand. *Inorg. Chem.* **2018**, *57*, 3720−3730.

(7) (a) Schaffner-Hamann, C.; von Zelewsky, A.; Barbieri, A.; Barigelletti, F.; Muller, G.; Riehl, J. P.; Neels, A. Diastereoselective Formation of Chiral Tris-Cyclometalated Iridium (III) Complexes: Characterization and Photophysical Properties. *J. Am. Chem. Soc.* **2004**, *126*, 9339−9348. (b) Haberhauer, G.; Oeser, T.; Rominger, F. A widely applicable concept for predictable induction of preferred configuration in C3-symmetric systems. *Chem. Commun.* **2005**, 2799−2801. (c) St-Pierre, G.; Ladouceur, S.; Fortin, D.; Zysman-Colman, E. Fraternal twin iridium hemicage chelates. *Dalton Trans.* **2011**, *40*, 11726−11731. (d) Moriuchi, T.; Mao, L.; Wu, H.-L.; Ohmura, S. D.; Watanabe, M.; Hirao, T. Synthesis of facial cyclometalated iridium-(III) complexes triggered by tripodal ligands. *Dalton Trans.* **2012**, *41*, 9519−9525.

(8) (a) Ruggi, A.; Alonso, M. B.; Reinhoudt, D. N.; Velders, A. H. An iridium(III)-caged complex with low oxygen quenching. *Chem. Commun.* **2010**, *46*, 6726−6728. (b) Sato, H.; Blemker, M. A.; Hellinghausen, G.; Armstrong, D. W.; Nafie, J. W.; Roberts, S. T.; Krische, M. J. Triple Helical Ir(ppy)3 Phenylene Cage Prepared by Diol-Mediated Benzannulation: Synthesis, Resolution, Absolute Stereochemistry and Photophysical Properties. *Chem.—Eur. J.* **2019**, *25*, 8719−8724.

(9) (a) Albrecht, M. Cyclometalation Using d-Block Transition Metals: Fundamental Aspects and Recent Trends. *Chem. Rev.* **2010**, *110*, 576−623. (b) Gyton, M. R.; Leforestier, B.; Chaplin, A. B. Rhodium(III) and Iridium(III) Complexes of a NHC-Based Macro-cycle: Persistent Weak Agostic Interactions and Reactions with Dihydrogen. *Organometallics* **2018**, *37*, 3963−3971. (c) Leforestier, B.; Gyton, M. R.; Chaplin, A. B. Synthesis and group 9 complexes of macrocyclic PCP and POCOP pincer ligands. *Dalton Trans.* **2020**, *49*, 2087−2101. (d) Wang, X.; Peng, T.; Nguyen, C.; Lu, Z.-H.; Wang, N.; Wu, W.; Li, Q.; Wang, S. Highly Efficient Deep-Blue Electrophosphorescent Pt(II) Compounds with Non-Distorted Flat Geometry: Tetradentate versus Macrocyclic Chelate Ligands. *Adv. Funct. Mater.* **2017**, *27*, 1604318. (e) Hahn, F. E.; Langenhahn, V.; Lügger, T.; Pape, T.; Van, D. L. Template Synthesis of a Coordinated Tetracarbene Ligand with Crown Ether Topology. *Angew. Chem., Int. Ed.* **2005**, *44*, 3759−3763. (f) Lu, Z.; Cramer, S. A.; Jenkins, D. M. Exploiting a dimeric silver transmetallating reagent to synthesize macrocyclic tetracarbene complexes. *Chem. Sci.* **2012**, *3*, 3081−3087. (g) Altmann, P. J.; Weiss, D. T.; Jandl, C.; Kühn, F. E. Exploring Coordination Modes: Late Transition Metal Complexes with a Methylene-bridged Macrocyclic Tetra-NHC Ligand. *Chem.—Asian J.* **2016**, *11*, 1597−1605. (h) Fei, F.; Lu, T.; Chen, X.-T.; Xue, Z.-L.

Synthesis and structural characterization of metal complexes with macrocyclic tetracarbene ligands. *New J. Chem.* **2017**, *41*, 13442−13453.

(10) (a) Liu, Z.; Nalluri, S. K. M.; Stoddart, J. F. Surveying Macrocyclic Chemistry: From Flexible Crown Ethers to Rigid Cyclophanes. *Chem. Soc. Rev.* **2017**, *46*, 2459−2478. (b) Haque, F. M.; Grayson, S. M. The synthesis, properties and potential applications of cyclic polymers. *Nat. Chem.* **2020**, *12*, 433−444. (c) Hua, B.; Shao, L.; Li, M.; Liang, H.; Huang, F. Macrocycle-Based Solid-State Supramolecular Polymers. *Acc. Chem. Res.* **2022**, *55*, 1025−1034.

(11) (a) Martí-Centelles, V.; Pandey, M. D.; Burguete, M. I.; Luis, S. V. Macrocyclization reactions: the importance of conformational, configurational, and template-induced preorganization. *Chem. Rev.* **2015**, *115*, 8736−8834. (b) Mortensen, K. T.; Osberger, T. J.; King, T. A.; Sore, H. F.; Spring, D. R. Strategies for the Diversity-Oriented Synthesis of Macrocycles. *Chem. Rev.* **2019**, *119*, 10288−10317. (c) Chaudhry, M. T.; Akine, S.; MacLachlan, M. J. Contemporary Macrocycles for Discrete Polymetallic Complexes: Precise Control Over Structure and Function. *Chem. Soc. Rev.* **2021**, *50*, 10713−10732.

(12) (a) Thompson, M. C.; Busch, D. H. Reactions of Coordinated Ligands. IX. Utilization of the Template Hypothesis to Synthesize Macrocyclic Ligands in Situ. *J. Am. Chem. Soc.* **1964**, *86*, 3651−3656. (b) Busch, D. H. First Considerations: Principles, Classification, and History. *Top. Curr. Chem.* **2005**, *249*, 1−65. (c) Meyer, C. D.; Joiner, C. S.; Stoddart, J. F. Template-directed synthesis employing reversible imine bond formation. *Chem. Soc. Rev.* **2007**, *36*, 1705−1723. (d) Fabbrizzi, L.; Licchelli, M.; Mosca, L.; Poggi, A. Template synthesis of azacyclam metal complexes using primary amides as locking fragments. *Coord. Chem. Rev.* **2010**, *254*, 1628−1636.

(13) (a) Pedersen, C. J. Cyclic polyethers and their complexes with metal salts. *J. Am. Chem. Soc.* **1967**, *89*, 7017−7036. (b) Christensen, J. J.; Hill, J. O.; Izatt, R. M. Ion Binding by Synthetic Macrocyclic Compounds: Selective ion binding in the interior of ring structures characterize these compounds. *Science* **1971**, *174*, 459−467.

(14) (a) Li, L.-P.; Peng, H.-L.; Wei, L.-Q.; Ye, B.-H. Diastereoselective Photooxidation and Reduction of Chiral Iridium-(III) Complexes. *Inorg. Chem.* **2019**, *58*, 785−793. (b) Peng, H.-L.; Li, Y.; Chen, X.-Y.; Li, L.-P.; Ke, Z.; Ye, B.-H. Visible-Light-Induced Amination of Quinoline at the C8 Position via a Postcoordinated Interligand-Coupling Strategy under Mild Conditions. *Inorg. Chem.* **2021**, *60*, 908−918. (c) Peng, H.-L.; Chen, X.-Y.; Li, L.-P.; Ye, B.-H. Mechanism study on photo-oxidation dehydrogenation of cyclo-metalated Ir(III) amino acid complexes. *Inorg. Chim. Acta* **2020**, *513*, No. 119939. (d) Xiong, M.-F.; Peng, H.-L.; Zhang, X.-P.; Ye, B.-H. Discrepancy between Proline and Homoproline in Chiral Recognition and Diastereomeric Photoreactivity with Iridium(III) Complexes. *Inorg. Chem.* **2021**, *60*, 5423−5431. (e) Xiong, M.-F.; Ye, B.-H. Regioselective Dehydrogenation of the Secondary Amine Complexes into Imine Complexes under Visible-Light Irradiation. *Organometallics* **2022**, *41*, 617−626. (f) Xiong, M.-F.; Zhou, H.-Y.; Huang, X.-K.; Fan, J.-Y.; Ye, B.-H. Chiral Recognition and Photoreaction of β-Amino Acids with Iridium(III) Complexes. *Chin. J. Chem.* **2022**, *40*, 2909−2918.

(15) (a) Chen, X.-Y.; Yao, S.-Y.; Li, L.-P.; Ye, B.-H. Diastereoselective photoreaction of Ir(III) amine complexes for generation new multidentate ligands in situ via a postcoordinated interligand coupling strategy. *Chin. J. Chem.* **2021**, *39*, 2995−3003. (b) Huang, X.-K.; Li, L.-P.; Zhou, H.-Y.; Xiong, M.-F.; Fan, J.-Y.; Ye, B.-H. Switching the Photoreactions of Ir(III) Diamine Complexes between C-N Coupling and Dehydrogenation under Visible Light Irradiation. *Inorg. Chem.* **2022**, *61*, 20834−20847. (c) Xiong, M.-F.; Liu, G.-F.; Ye, B.-H. Solvent-Induced Umpolung Reaction from Dioxygenation to C-S Coupling in Bis(2-phenylquinoline) Iridium(III) Thiolate Complexes. *Inorg. Chem.* **2023**, *62*, 11654−11664.

(16) Dong, J.; Guo, H.; Hu, Q. S. Room Temperature Ni0/PCy3-Catalyzed Coupling Reactions of Aryl Arenesulfonates with Bis-(pinacolato)diboron. *Eur. J. Org. Chem.* **2017**, *2017*, 7087−7090.

(17) Barefield, E. K.; Wagner, F.; Hodges, K. D. Synthesis of macrocyclic tetramines by metal ion assisted cyclization reactions. *Inorg. Chem.* **1976**, *15*, 1370−1377.

(18) (a) Chen, C.; Hong, S. H. Selective Catalytic sp³ C-O Bond Cleavage with C-N Bond Formation in 3-Alkoxy-1-propanols. *Org. Lett.* **2012**, *14*, 2992−2995. (b) Do, L. H.; Lippard, S. J. Toward functional carboxylate-bridged diiron protein mimics: achieving structural stability and conformational flexibility using a macrocyclic ligand framework. *J. Am. Chem. Soc.* **2011**, *133*, 10568−10581.

(19) (a) Ishiyama, T.; Murata, M.; Miyaura, N. Palladium(0)-Catalyzed Cross-Coupling Reaction of Alkoxydiboron with Haloarenes: A Direct Procedure for Arylboronic Esters. *J. Org. Chem.* **1995**, *60*, 7508−7510. (b) Delaney, C. P.; Kassel, V. M.; Denmark, S. E. Potassium Trimethylsilanolate Enables Rapid, Homogeneous Suzuki-Miyaura Cross-Coupling of Boronic Esters. *ACS Catal.* **2020**, *10*, 73−80.

(20) (a) Matsuo, N. Benzo[h]quinolin-10-yl-N Iridium(III) Complexes. *Bull. Chem. Soc. Jpn.* **1974**, *47*, 767−768. (b) Yao, S.-Y.; Ou, Y. L.; Ye, B.-H. Asymmetric Synthesis of Enantiomerically Pure Mono- and Binuclear Bis(cyclometalated) Iridium(III) Complexes. *Inorg. Chem.* **2016**, *55*, 6018−6026. (c) Li, L.-P.; Yao, S.-Y.; Ou, Y.-L.; Wei, L.-Q.; Ye, B.-H. Diastereoselective Synthesis and Photophysical Properties of Bis-Cyclometalated Ir(III) Stereoisomers with Dual Stereocenters. *Organometallics* **2017**, *36*, 3257−3265.

(21) Gitlina, A. Y.; Khistiaeva, V.; Melnikov, A.; Ivonina, M.; Sizov, V.; Spiridonova, D.; Makarova, A.; Vyalikh, D.; Grachova, E. Organometallic Ir(III) complexes: post-synthetic modification, photophysical properties and binuclear complex construction. *Dalton Trans.* **2023**, *52*, 8986−8997.

(22) (a) Mitra, R.; Zhu, H.; Grimme, S.; Niemeyer, J. Functional Mechanically Interlocked Molecules: Asymmetric Organocatalysis with a Catenated Bifunctional Bronsted Acid. *Angew. Chem., Int. Ed. Engl.* **2017**, *56*, 11456−11459. (b) Dopp, C. M.; Golwankar, R. R.; Kelsey, S. R.; Douglas, J. T.; Erickson, A. N.; Oliver, A. G.; Day, C. S.; Day, V. W.; Blakemore, J. D. Vanadyl as a Spectroscopic Probe of Tunable Ligand Donor Strength in Bimetallic Complexes. *Inorg. Chem.* **2023**, *62*, 9827−9843.

(23) (a) Blakemore, J. D.; Chitta, R.; D'Souza, F. Synthesis and study of crown ether-appended boron dipyrrin chemosensors for cation detection. *Tetrahedron Lett.* **2007**, *48*, 1977−1982. (b) Rodriguez, J. D.; Lisy, J. M. Probing ionophore selectivity in argon-tagged hydrated alkali metal ion-crown ether systems. *J. Am. Chem. Soc.* **2011**, *133*, 11136−11146.

(24) (a) Lamansky, S.; Djurovich, P.; Murphy, D.; Abdel-Razzaq, F.; Lee, H.-E.; Adachi, C.; Burrows, P. E.; Forrest, S. R.; Thompson, M. E. Highly Phosphorescent Bis-Cyclometalated Iridium Complexes: Synthesis, Photophysical Characterization, and Use in Organic Light Emitting Diodes. *J. Am. Chem. Soc.* **2001**, *123*, 4304−4312. (b) Ma, D.; Liu, R.; Qiu, Y.; Duan, L. High-performance yellow and orange-emitting diodes based on novel sublimable cationic iridium(III) complexes by ligand control. *J. Mater. Chem. C* **2018**, *6*, 5630−5638. (c) Yoon, S.; Gray, T. G.; Teets, T. S. Enhanced Deep-Red Phosphorescence in Cyclometalated Iridium Complexes with Quinoline-Based Ancillary Ligands. *Inorg. Chem.* **2023**, *62*, 7898−7905.

(25) (a) Gollnick, K.; Schenck, G. O. Mechanism and stereoselectivity of photosensitized oxygen transfer reactions. *Pure Appl. Chem.* **1964**, *9*, 507−525. (b) Monroe, B. M. Rate Constants for the Reaction of Singlet Oxygen with Conjugated Dienes. *J. Am. Chem. Soc.* **1981**, *103*, 7253−7256. (c) Murasecco-Suardi, P.; Gassmann, E.; Braun, A. M.; Oliveros, E. Determination of the Quantum Yield of Intersystem Crossing of Rose Bengal. *Helv. Chim. Acta* **1987**, *70*, 1760−1773. (d) Li, Z. Z.; Niu, Y. L.; Zhou, H. Y.; Chao, H. Y.; Ye, B.-H. Visible-light-induced photooxidation of ruthenium(II) complex with 2,2′-biimidazole-like ligand by singlet oxygen. *Inorg. Chem.* **2013**, *52*, 10087−10095.

(26) (a) Mellah, M.; Voituriez, A.; Schulz, E. Chiral Sulfur Ligands for Asymmetric Catalysis. *Chem. Rev.* **2007**, *107*, 5133−5209. (b) Wojaczyńska, E.; Wojaczyński, J. Enantioselective Synthesis of Sulfoxides: 2000−2009. *Chem. Rev.* **2010**, *110*, 4303−4356. (c) Sipos,

G.; Drinkel, E. E.; Dorta, R. The Emergence of Sulfoxides as Efficient Ligands in Transition Metal Catalysis. *Chem. Soc. Rev.* **2015**, *44*, 3834−3860. (d) Bentley, R. Role of Sulfur Chirality in the Chemical Processes of Biology. *Chem. Soc. Rev.* **2005**, *34*, 609−624. (e) Nishiguchi, S.; Izumi, T.; Kouno, T.; Sukegawa, J.; Ilies, L.; Nakamura, E. Synthesis of Esomeprazole and Related Proton Pump Inhibitors through Iron-Catalyzed Enantioselective Sulfoxidation. *ACS Catal.* **2018**, *8*, 9738−9743.

(27) (a) Zen, J.-M.; Liou, S.-L.; Kumar, A. S.; Hsia, M.-S. An Efficient and Selective Photocatalytic System for the Oxidation of Sulfides to Sulfoxides. *Angew. Chem., Int. Ed.* **2003**, *42*, 577−579. (b) Jiang, J.; Luo, R.; Zhou, X.; Chen, Y.; Ji, H. Photocatalytic Properties and Mechanistic Insights into Visible Light-Promoted Aerobic Oxidation of Sulfides to Sulfoxides via Tin Porphyrin-Based Porous Aromatic Frameworks. *Adv. Synth. Catal.* **2018**, *360*, 4402−4411.

(28) Li, C. J. Organic Reactions in Aqueous Media with a Focus on Carbon-Carbon Bond Formations: A Decade Update. *Chem. Rev.* **2005**, *105*, 3095−3166.

(29) (a) Miller, B. L.; Williams, T. D.; Schöneich, C. Mechanism of Sulfoxide Formation through Reaction of Sulfur Radical Cation Complexes with Superoxide or Hydroxide Ion in Oxygenated Aqueous Solution. *J. Am. Chem. Soc.* **1996**, *118*, 11014−11025. (b) Xing, C.; Deng, J.; Tan, R.; Gao, M.; Hao, P.; Yin, D.; Yin, D. Cooperative Chiral Salen Ti^{IV} Catalyst Supported on Ionic Liquid-Functionalized Graphene Oxide Accelerates Asymmetric Sulfoxidation in Water. *Catal. Sci. Technol.* **2017**, *7*, 5944−5952. (c) Heydari-turkmani, A.; Zakavi, S. The First Solid State Porphyrin-Weak Acid Molecular Complex: A Novel Metal Free, Nanosized and Porous Photocatalyst for Large Scale Aerobic Oxidations in Water. *J. Catal.* **2018**, *364*, 394−405. (d) Wei, L.-Q.; Ye, B.-H. Cyclometalated Ir−Zr Metal−Organic Frameworks as Recyclable Visible-Light Photocatalysts for Sulfide Oxidation into Sulfoxide in Water. *ACS Appl. Mater. Interfaces* **2019**, *11*, 41448−41457.

(30) (a) Gao, R.; Ho, D. G.; Hernandez, B.; Selke, M.; Murphy, D.; Djurovich, P. I.; Thompson, M. E. Bis-cyclometalated Ir(III) complexes as efficient singlet oxygen sensitizers. *J. Am. Chem. Soc.* **2002**, *124*, 14828−14829. (b) Sun, J.; Zhong, F.; Yi, X.; Zhao, J. Efficient Enhancement of the Visible-Light Absorption of Cyclometalated Ir(III) Complexes Triplet Photosensitizers with Bodipy and Applications in Photooxidation and Triplet Triplet Annihilation Upconversion. *Inorg. Chem.* **2013**, *52*, 6299−6310. (c) Li, L.-P.; Ye, B.-H. Efficient Generation of Singlet Oxygen and Photooxidation of Sulfide into Sulfoxide via Tuning the Ancillary of Bicyclometalated Iridium(III) Complexes. *Inorg. Chem.* **2019**, *58*, 7775−7784.

(31) (a) Bonesi, S. M.; Manet, I.; Freccero, M.; Fagnoni, M.; Albini, A. Photosensitized Oxidation of Sulfides: Discriminating between the Singlet-Oxygen Mechanism and Electron Transfer Involving Superoxide Anion or Molecular Oxygen. *Chem.—Eur. J.* **2006**, *12*, 4844−4857. (b) Baptista, M. S.; Cadet, J.; Di Mascio, P.; Ghogare, A. A.; Greer, A.; Hamblin, M. R.; Lorente, C.; Nunez, S. C.; Ribeiro, M. S.; Thomas, A. H.; Vignoni, M.; Yoshimura, T. M. Type I and Type II Photosensitized Oxidation Reactions: Guidelines and Mechanistic Pathways. *Photochem. Photobiol.* **2017**, *93*, 912−919.

(32) (a) Baciocchi, E.; Giacco, T. D.; Elisei, F.; Gerini, M. F.; Guerra, M.; Lapi, A.; Liberali, P. Electron Transfer and Singlet Oxygen Mechanisms in the Photooxygenation of Dibutyl Sulfide and Thioanisole in MeCN Sensitized by N-Methylquinolinium Tetrafluoborate and 9,10-Dicyanoanthracene. The Probable Involvement of a Thiadioxirane Intermediate in Electron Transfer Photooxygenations. *J. Am. Chem. Soc.* **2003**, *125*, 16444−16454. (b) Jensen, F. Reaction of Organic Sulfides with Singlet Oxygen. A Theoretical Study Including Electron Correlation. *J. Org. Chem.* **1992**, *57*, 6478−6487. (c) Jensen, F.; Greer, A.; Clennan, E. L. Reaction of Organic Sulfides with Singlet Oxygen. A Revised Mechanism. *J. Am. Chem. Soc.* **1998**, *120*, 4439−4449.